Problems with Ultrahigh-energy Neutrino Interactions[1]

Dieter Schildknecht[2]

Fakultät für Physik, Universität Bielefeld,
Universitätsstraße 25, 33615 Bielefeld, Germany
and
Max-Planck-Institute for Physics, Föhringer Ring 6,
80805 Munich, Germany

arXiv:1411.0498v1 [hep-ph] 3 Nov 2014

Abstract

The IceCube collaboration has recently identified events due to ultrahigh-energy neutrino interactions. Predictions of the neutrino-nucleon cross section at ultrahigh energies require a huge extrapolation of the cross sections experimentally measured at laboratory energies. Upon relating neutrino scattering to deep inelastic electron scattering, we show that the empirically verified color dipole picture is well suited for such an extrapolation. The dominant contribution to the total neutrino-nucleon cross section, even at ultrahigh energies, is due to the kinematic range where color transparency is valid for the color dipole interaction. We deviate from various claims in the literature on the presence of screening effects due to non-linear evolution at ultrahigh neutrino energies.

1 The IceCube Experiment

The IceCube experiment, located at the South Pole, covers a cubic kilometer of Antarctic glacial ice. It detects neutrinos by observing Cherenkov light from secondary charged particles produced in neutrino-nucleon interactions. In 2013, the IceCube collaboration announced the detection of 28 neutrino events of ultra-high energy:

- 26 events in the energy range of 50 TeV to 1 PeV = 10^{15} eV,
- 2 events in the energy range of 1 PeV to 2 PeV,
- zero events above 2 PeV.

In fig. 1, I show the flux (e.g. [1]) of cosmic rays. The ultrahigh energies of the observed neutrino events are significantly below the upper end of the energy spectrum of cosmic rays.

[1]Presented at the International School of Subnuclear Physics, 52nd Course, Erice-Sicily, 24 June - 3 July 2014

[2]Email: schild@physik.uni-bielefeld.de

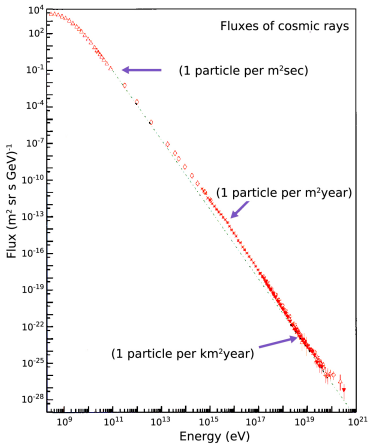

Figure 1: Flux of cosmic rays as a function of their energy.

A recent, eighty-page review paper, entitled "Cosmic Neutrino Pevatrons: A Brand New Pathway to Astronomy, Astrophysics, and Particle Physics" [2], contains a thorough discussion on the interpretation of the IceCube events. It covers potential sources of the neutrino events, galactic and extragalactic ones, as well as probes of fundamental physics. Cosmic probes include e.g. superheavy Dark Matter, lepto-quarks produced via $\nu_\tau + q \to LQ \to \tau + q$, and others.

Let me only mention a single recent speculative remark [3] on the possibility of an exotic neutrino property. The suggestion is as simple, as it is far reaching at the same time. The afore-mentioned energies of the IceCube events (in distinction from the upper end of the cosmic-ray flux in fig. 1) do not extend beyond approximately 2 PeV. In particular, the enhancement of the neutrino signal due to the so-called Glashow resonance [4]

$$\nu_e e^- \to W^- \to \text{anything},$$

corresponding to an energy of about $E \simeq 6.3$ PeV in the rest frame of the interacting electron e^-, has not been observed (up to now). Interpreting this non-observation as the consequence of a strict universal bound on the neutrino energy, E^ν_{Max}, located below 6.3 PeV, from

$$E^\nu_{Max} = \frac{m_\nu}{\sqrt{1-\beta^2_\nu}} = \gamma_\nu m_\nu,$$

one concludes that $\gamma_\nu = E^\nu_{Max}/m_\nu < \infty$ with the dramatic consequence of a violation of Lorentz invariance for neutrinos.

With respect to future searches for, and for the detailed analysis of ultrahigh-energy neutrino events, a knowledge of the neutrino-nucleon cross section is indispensable. Predictions of the cross section for ultrahigh energies of neutrinos require huge extrapolations to energies far beyond the energies where experimental data from laboratory experiments are available. The highest energies in laboratory experiments on lepton scattering were reached for charged-lepton scattering at the electron-proton collider HERA in Hamburg, which was running during the years from 1990 to 2007. By relating neutrino scattering to charged-lepton scattering, the HERA experimental data can be used as a reliable base for the extrapolation to the ultrahigh energies observed for cosmic neutrinos.

2 The Neutrino-Nucleon Cross Section at Ultrahigh Energies.

2.1 Connection to Deep Inelastic Electron-Nucleon Scattering.

The total charged-current neutrino-nucleon cross section is given by (e.g. [5])

$$\sigma_{\nu N}(E) = \frac{G_F^2}{2\pi} \int_{Q^2_{min.}}^{s-M_p^2} dQ^2 \left(\frac{M_W^2}{Q^2 + M_W^2} \right)^2 \int_{M_p^2}^{s-Q^2} \frac{dW^2}{W^2} \sigma_r(x, Q^2). \tag{2.1}$$

In (2.1), E denotes the neutrino energy in the nucleon rest frame. It is related to the neutrino-nucleon center-of-mass energy by

$$s = 2M_p E + M_p^2 \cong 2M_p E, \tag{2.2}$$

where M_p denotes the proton mass. The integrations in (2.1) run over the four-momentum-transfer squared from the neutrino to the nucleon, Q^2, and the square of the total energy, W^2, of the produced hadronic system. The Fermi coupling is denoted by G_F, and the W-boson mass by M_W. The reduced cross section, $\sigma_r(x, Q^2)$ in (2.1), depends on the three nucleon structure functions $F^{\nu N}_{2,L,3}(x, Q^2)$,

$$\sigma_r(x, Q^2) = \frac{1 + (1-y)^2}{2} F_2^{\nu N}(x, Q^2) - \frac{y^2}{2} F_L^{\nu N}(x, Q^2) + y(1 - \frac{y}{2}) x F_3^{\nu N}(x, Q^2), \tag{2.3}$$

where x is the Bjorken variable,

$$x = \frac{Q^2}{2qP} = \frac{Q^2}{W^2 + Q^2 - M_p^2} \cong \frac{Q^2}{W^2}, \tag{2.4}$$

and y denotes the squared fraction of the total neutrino energy producing hadrons in the final state

$$y = \frac{Q^2}{2M_p E x} \cong \frac{W^2}{s}. \tag{2.5}$$

According to (2.1), at ultra-high energies, $s \gg M_W^2$, the contribution to the total cross section due to $Q^2 \gg M_W^2$ is strongly suppressed. The dominant contribution to the cross section is due to $Q^2 \cong M_W^2$ and due to small values of $x \cong M_W^2/s \ll 0.1$.

At low values of $x \lesssim 0.1$, neutrino-nucleon and electron-nucleon interactions proceed via fluctuations of the virtual W-boson and virtual photon, respectively, into quark-antiquark pairs that propagate and interact via gluon exchange with the nucleon. For a given number of n_f actively contributing quark flavors, the flavor-independent QCD interaction implies the proportionality

$$\frac{1}{n_f} F_{2,L}^{\nu N}(x, Q^2) = \frac{1}{\sum_q Q_q^2} F_{2,L}^{eN}(x, Q^2). \tag{2.6}$$

It allows to predict the neutrino-nucleon structure functions, $F_{2,L}^{\nu N}(x, Q^2)$, from the electron-nucleon structure functions, $F_{2,L}^{eN}(x, Q^2)$. For $n_f = 4$ flavors, the proportionality factor in (2.6) becomes $n_f / \sum_q^{n_f} Q_q^2 = 5/18$.

The dominant term in (2.3) is due to $F_2^{\nu N}(x,Q^2)$. In what follows, we shall frequently use the relation between the proton structure function, $F_2^{ep}(x,Q^2)$, and the (virtual) photoabsorption cross section, $\sigma_{\gamma^* p}(W^2,Q^2)$, that, for $x \ll 0.1$, is given by

$$F_2^{ep}(x,Q^2) = \frac{Q^2}{4\pi^2\alpha}\sigma_{\gamma^* p}(W^2,Q^2). \tag{2.7}$$

2.2 Electron-Proton Deep Inelastic Scattering, Experimental Results.

As noted, neutrino scattering at ultrahigh energies is dominantly due to interactions in the kinematic range of $x \ll 0.1$. This is the region of the kinematic variables Q^2 and W^2, where the HERA experimental results show scaling in the low-x scaling variable [6],

$$\eta(W^2,Q^2) \equiv \frac{Q^2+m_0^2}{\Lambda^2_{sat}(W^2)}, \qquad \Lambda^2_{sat}(W^2) \sim (W^2)^{C_2} \tag{2.8}$$

i.e.

$$\sigma_{\gamma^* p}(W^2,Q^2) = \sigma_{\gamma^* p}(\eta(W^2,Q^2)) \sim \sigma^{(\infty)} \begin{cases} \frac{1}{\eta(W^2,Q^2)} & , \quad \text{for } \eta(W^2,Q^2) \gg 1, \\ \ln\frac{1}{\eta(W^2,Q^2)} & , \quad \text{for } \eta(W^2,Q^2) \ll 1. \end{cases} \tag{2.9}$$

The photoabsorption cross section, in the approximation where the (hadronic) cross section $\sigma^{(\infty)}(W^2) = \sigma^{(\infty)} \cong const$, depends on the single scaling variable $\eta(W^2,Q^2)$ defined in (2.8). Compare fig. 2.

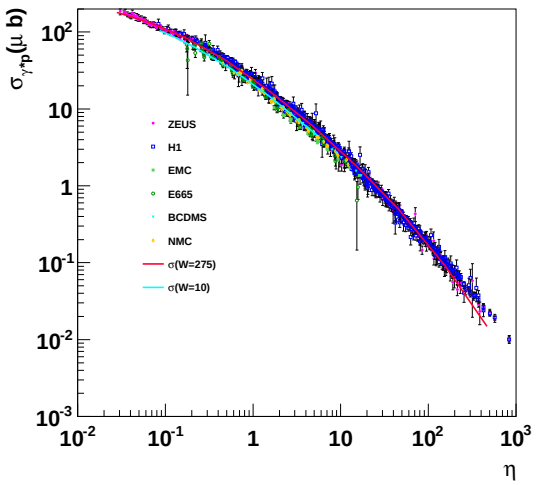

Figure 2: The total photoabsorption cross section as a function of the low-x scaling variable [6] $\eta \equiv \eta(W^2,Q^2)$.

The "saturation scale", $\Lambda^2_{sat}(W^2)$, grows as $\Lambda^2_{sat}(W^2) \sim (W^2)^{C_2}$, where $C_2 \simeq 0.3$, and the constant m_0, as expected from quark-hadron duality [7] for light quarks, is somewhat smaller than the ρ^0-meson mass, m_{ρ^0}. The functional dependence (2.9) of the photoabsorption cross section on $\eta(W^2,Q^2)$ can be read off from fig. 2.

We remark that the theoretical curves in fig. 2 were obtained in the color-dipole picture (CDP) to be discussed in the next section. The slight spread in the predictions for $W = 275$ GeV and $W = 10$ GeV, also visible in the experimental data, is due to the deviation of $\sigma^{(\infty)}(W^2)$ in (2.9) from $\sigma^{(\infty)}(W^2) = \sigma^{(\infty)} = \text{const.}$

The significant differences in the $\eta(W^2, Q^2)$ dependence for $\eta(W^2, Q^2) \gg 1$ and $\eta(W^2, Q^2) \ll 1$ in fig. 2 suggest a subdivision of the (Q^2, W^2) plane into (only and precisely) two regions subdivided by $\eta(W^2, Q^2) = 1$, compare fig. 3.

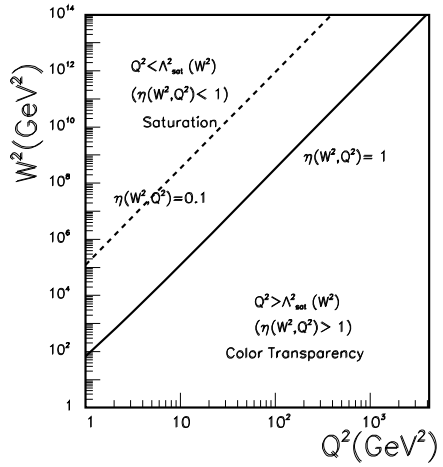

Figure 3: The (Q^2, W^2) plane with the line $\eta(W^2, Q^2) = 1$ separating the large-Q^2 color-transparency region from the saturation domain.

The logarithmic dependence of $\sigma_{\gamma^* p}(\eta(W^2, Q^2))$ for $\eta(W^2, Q^2) < 1$ implies the important limiting behavior [6, 8],

$$\lim_{\substack{W^2\to\infty \\ Q^2 \text{ fixed}}} \frac{\sigma_{\gamma^* p}(\eta(W^2, Q^2))}{\sigma_{\gamma^* p}(\eta(W^2, Q^2 = 0))} = \lim_{\substack{W^2\to\infty \\ Q^2 \text{ fixed}}} \frac{\ln\left(\frac{\Lambda^2_{sat}(W^2)}{m_0^2}\frac{m_0^2}{(Q^2+m_0^2)}\right)}{\ln\frac{\Lambda^2_{sat}(W^2)}{m_0^2}}$$
$$= 1 + \lim_{\substack{W^2\to\infty \\ Q^2 \text{ fixed}}} \frac{\ln\frac{m_0^2}{Q^2+m_0^2}}{\ln\frac{\Lambda^2_{sat}(W^2)}{m_0^2}} = 1. \qquad (2.10)$$

For $W^2 \to \infty$, and any fixed value of the photon virtuality, Q^2, the ratio of the photoabsorption cross section, $\sigma_{\gamma^* p}(\eta(W^2, Q^2))$, to the $Q^2 = 0$ photoproduction cross section $\sigma_{\gamma p}(W^2) \equiv \sigma_{\gamma^* p}(\eta(W^2, Q^2 = 0))$, becomes equal to unity. The photoabsorption cross section "saturates" to a unique limit that coincides with the hadronlike $Q^2 = 0$ photoproduction cross section.

The scaling behavior of $\sigma_{\gamma^* p}(\eta(W^2, Q^2)) \sim 1/\eta(W^2, Q^2)$ for $\eta(W^2, Q^2) \gg 1$, in terms of the proton structure function $F_2 \equiv F_2^{ep}(x, Q^2)$ at sufficiently large Q^2, corresponds to a single curve in the plot of the experimental data for F_2 against the variable $1/W^2$. The theoretical curve in fig. 4 is based on [9]

$$F_2(W^2) = f_2 \cdot \left(\frac{W^2}{1\text{GeV}^2}\right)^{C_2=0.29}, \qquad (2.11)$$

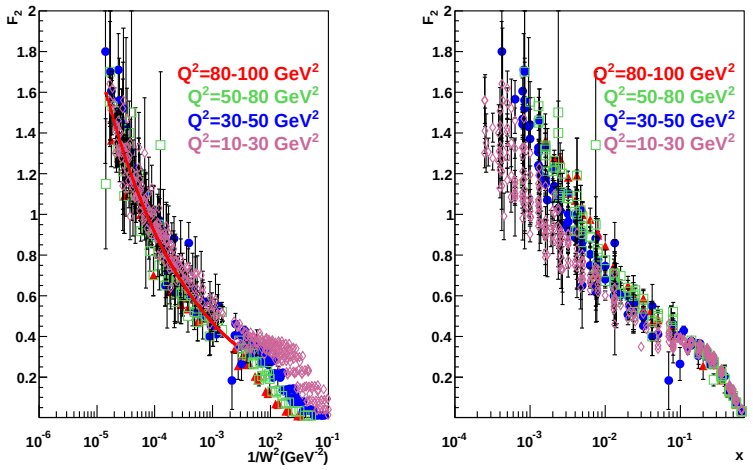

Figure 4: Experimental results for the proton structure function $F_2 \equiv F_2^{ep}(x, Q^2)$ as a function of $1/W^2$ and as a function of $1/x$ [9].

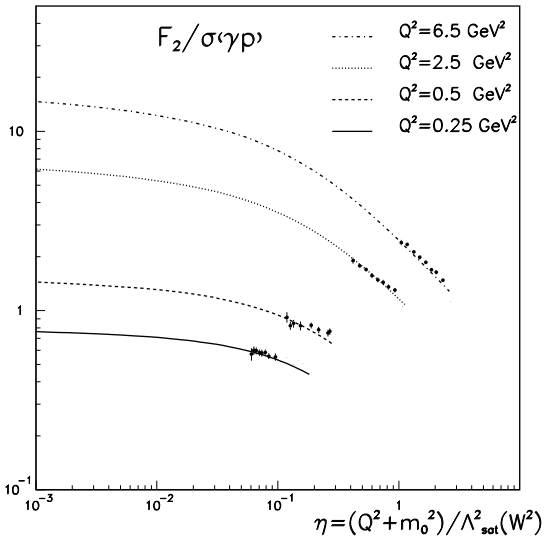

Figure 5: The approach to the saturation limit [9]. With decreasing $\eta(W^2, Q^2)$, the proton structure function $F_2(x, Q^2)$ approaches the saturation limit given by $Q^2\sigma_{\gamma p}(W^2)$, where $\sigma_{\gamma p}(W^2)$ denotes the $(Q^2 = 0)$ photoabsorption cross section.

where $f_2 = 0.063$. For comparison, in fig. 4, we also show F_2 as a function of the Bjorken variable x for fixed values of Q^2.

The transition to the saturation limit for $\eta(W^2, Q^2) \ll 1$, based on the CDP [9] is illustrated in fig. 5. Even for values of Q^2 as small as $Q^2 \cong 1\text{GeV}^2$, a strict and detailed empirical verification of the saturation limit requires "ultrahigh" energies far beyond the energies that were available at HERA.

The afore-mentioned experimental results on low-x DIS find a coherent *qualitative as well as quantitative* explanation in the color dipole picture (CDP) to which we shall turn next.

2.3 The Color Dipole Picture: Theory

In DIS at low $x \lesssim 0.1$, the photon virtually dissociates (or "fluctuates" in modern jargon) into hadronic vector states that subsequently interact with the nucleon (generalized vector dominance (GVD) [10], [11]). In QCD, the hadronic vector states are quark-antiquark ($q\bar{q}$) color-dipole states, which interact with the gluon field in the nucleon. Compare fig. 6 for the imaginary part of the associated forward-Compton-scattering amplitude.

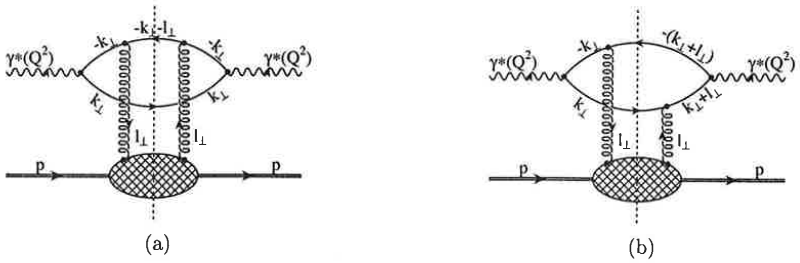

Figure 6: Two of the four diagrams for the $q\bar{q}$ dipole interaction with the gluon field in the nucleon. The diagrams (a) and (b) correspond to channel 1 and channel 2 respectively.

In terms of the transverse size, $\vec{r}_\perp$, of the $q\bar{q}$ pair, and the partition $0 \leq z \leq 1$ of the longitudinal momenta of quark and antiquark, the photoabsorption cross section, $\sigma_{\gamma^*_{L,T}p}(W^2, Q^2)$, for longitudinally and transversely polarized photons takes the form [12, 13]

$$\begin{aligned} \sigma_{\gamma^*_{L,T}p}(W^2, Q^2) &= \int dz \int d^2\vec{r}_\perp |\psi_{L,T}(\vec{r}_\perp, z(1-z), Q^2)|^2 \\ &\times \sigma_{(q\bar{q})p}(\vec{r}_\perp, z(1-z), W^2). \end{aligned} \tag{2.12}$$

The integrand in the photoabsorption cross section (2.12) shows the afore-mentioned factorization into the Q^2-dependent probability for a $\gamma^* \to q\bar{q}$ fluctuation and the W-dependent $(q\bar{q})p$ interaction cross section.

The gauge-invariant two-gluon interaction of the $q\bar{q}$ color-dipole state requires the representation [12, 13]

$$\sigma_{(q\bar{q})p}(\vec{r}_\perp, z(1-z), W^2) = \int^{\vec{l}_\perp^{\,2}{}_{Max}(W^2)} d^2\vec{l}_\perp \tilde{\sigma}\left(\vec{l}_\perp^{\,2}, z(1-z), W^2\right)\left(1 - e^{-i\vec{l}_\perp \vec{r}_\perp}\right). \tag{2.13}$$

The CDP, accordingly, rests on the general form (2.12) of the photoproduction cross section at low x, combined with the constraint on the dipole cross section (2.13)[3]

Employing the explicit (QED) expression for the $\gamma^* \to q\bar{q}$ transition probability, the photoabsorption cross section (2.12) may be written as [9]

$$\sigma_{\gamma^*_{L,T}p}(W^2, Q^2) = \frac{\alpha}{\pi} \sum_q Q_q^2 Q^2 \int dr'^2_\perp K^2_{0,1}(r'_\perp Q) \sigma_{(q\bar{q})^{J=1}_{L,T}p}(r'^2_\perp, W^2). \tag{2.14}$$

[3]We stress the dependence of the dipole cross section (2.13) on the energy W, [10], [13], [6], [11], [14] as implied by the fluctuation of the photon into on-shell $q\bar{q}$ dipole states, forbidding the Q^2 dependence (via Bjorken $x \sim Q^2/W^2$ dependence) frequently assumed in the literature.

In the transition from (2.12) to (2.14), massless quarks were assumed, and, by the appropriate projection, the cross sections $\sigma_{(q\bar{q})^{J=1}_{L,T}p}(r'^2_\perp, W^2)$ for the scattering of $(q\bar{q})^{J=1}_{L,T}$ states were introduced. The sum $\sum_q Q_q^2$ in (2.14) runs over the actively contributing quark flavors, and $K_0(r'_\perp Q)$ and $K_1(r'_\perp Q)$ denote modified Bessel functions. In terms of the $J = 1$ projections, $\sigma_{(q\bar{q})^{J=1}_{L,T}p}(r'_\perp, W^2)$, of the dipole cross section in (2.12), the two-gluon structure of the dipole cross section from (2.13) becomes [9]

$$\sigma_{(q\bar{q})^{J=1}_{L,T}p}(r'_\perp, W^2) = \pi \int d\vec{l}'^2_\perp \bar{\sigma}_{(q\bar{q})^{J=1}_{L,T}p}(\vec{l}'^2_\perp, W^2) \left(1 - \frac{\int d\vec{l}'^2_\perp \bar{\sigma}_{(q\bar{q})^{J=1}_{L,T}p}(\vec{l}'^2_\perp, W^2) J_0(l'_\perp r'_\perp)}{\int d\vec{l}'^2_\perp \bar{\sigma}_{(q\bar{q})^{J=1}_{L,T}p}(\vec{l}'^2_\perp, W^2)} \right), \tag{2.15}$$

where $J_0(l'_\perp r'_\perp)$ is the Bessel function with index 0.

The representation of the photoabsorption cross section (2.14) together with the constraint (2.15) allows one to *derive* [9], [15] the important *qualitative* behavior of the photoabsorption cross section (2.9) seen in the experimental data in fig. 2.

For any fixed value of Q^2, the strong decrease of the functions $K^2_{0,1}(r'_\perp Q)$ restricts the range of $r'_\perp$ relevant for the integration over the dipole size $r'^2_\perp$ in (2.14). The behavior of the dipole cross section in (2.14) for this Q^2-dependent effective dipole size $r'^2_\perp$, limited according to (2.15), is determined by the interaction energy, W, of the $q\bar{q}$ dipole state. Assuming that the effective upper limit of the integration over $d\vec{l}'^2_\perp$ in (2.15), given by $\vec{l}'^2_{\perp Max}(W^2)$, increases with the energy W, two different limiting behaviors of the dipole cross section at a fixed value of $r'_\perp$ can be discriminated.

For the case of relatively low energy, namely for $0 < l'_\perp r'_\perp < l'_{\perp Max}(W^2) r'_\perp \ll 1$, the expansion of the Bessel function in (2.15) implies that the dipole-proton cross section (2.15) vanishes proportional to the dipole size squared ("color transparency" limit),

$$\sigma_{(q\bar{q})^{J=1}_{L,T}p}(r'^2_\perp, W^2) \sim r'^2_\perp. \tag{2.16}$$

The proportionality factor in (2.16) is given by the first moment of $\bar{\sigma}_{(q\bar{q})^{J=1}_{L,T}p}(\vec{l}'^2_\perp, W^2)$, and is identified with the saturation scale $\Lambda^2_{sat}(W^2)$ introduced in (2.8).

For the case of very high energy, such that $l'^2_{\perp Max}(W^2) r' \gg 1$, rapid oscillations of the Bessel function $J_0(l'_\perp r'_\perp)$ in (2.15) imply ("saturation" limit).

$$\lim_{\substack{r'^2 fixed \\ W^2 \to \infty}} \sigma_{(q\bar{q})^{J=1}_{L,T}p}(r'^2_\perp, W^2) = \lim_{\substack{r'^2_\perp \to \infty \\ W^2 = const}} \sigma_{(q\bar{q})^{J=1}_{L,T}p}(r'^2_\perp, W^2) = \sigma^{(\infty)}_{L,T}(W^2). \tag{2.17}$$

At fixed dipole size, for W^2 sufficiently large the dipole cross section converges to the hadronic cross section that at most depends weakly on W^2, i.e. $\sigma^{(\infty)}_{L,T}(W^2) \simeq \sigma^{(\infty)} = \text{const}$.

Evaluating the photoabsorption cross section (2.12) for the two different limits, (2.16) and (2.17), we find [9, 15]

$$\begin{aligned} \sigma_{\gamma^* p}(W^2, Q^2) &= \sigma_{\gamma^* p}(\eta(W^2, Q^2)) \\ &= \frac{\alpha}{\pi} \sum_q Q_q^2 \begin{cases} \frac{1}{6}(1+2\rho)\sigma^{(\infty)}_L(W^2) \frac{1}{\eta(W^2,Q^2)} & , \quad (\eta(W^2,Q^2) \gg 1) \\ \sigma^{(\infty)}_T(W^2) \ln \frac{1}{\eta(W^2,Q^2)} & , \quad (\eta(W^2,Q^2) \ll 1) \end{cases} \end{aligned} \tag{2.18}$$

The form (2.18) agrees with the empirical result (2.9)[4]. The form of the $q\bar{q}$ color-dipole interaction (2.13) dictated by gauge invariance, *implies scaling* in $\eta(W^2, Q^2)$ of the total photoabsorption cross section. The empirical functional dependence, as $1/\eta(W^2, Q^2)$ and as $\ln(1/\eta(W^2, Q^2))$ in (2.9), is traced back to *color transparency and saturation* of the $(q\bar{q})p$ color dipole interaction.

2.4 A Remark on the Gluon Distribution.

The proton structure function in the CDP, according to (2.18) as well as (2.11) and fig. 4, is given by

$$F_2^{ep}(x, Q^2) \sim \begin{cases} \sigma^{(\infty)} \Lambda^2_{sat}(W^2) & , \quad (\eta(W^2, Q^2) \gg 1) \\ Q^2 \sigma^{(\infty)} \ln \frac{\Lambda^2_{sat}(W^2)}{Q^2 + m_0^2} & , \quad (\eta(W^2, Q^2) \ll 1) \end{cases} \tag{2.19}$$

Noting that in the perturbative-QCD-improved parton model the structure function $F_2^{ep}(x, Q^2)$ is proportional to the gluon-distribution function, we have to identify [9]

$$\sigma^{(\infty)}(W^2) \Lambda^2_{sat}(W^2) \sim \alpha_s(Q^2) x g(x, Q^2)|_{x=\frac{Q^2}{W^2}} . \tag{2.20}$$

The W dependence of the structure function, $F_2^{ep}(x, Q^2)$ at large values of $\eta(W^2, Q^2) \gg 1$, compare (2.19) and fig. 4, implies that the gluon structure function depends on the single variable W^2. Since the CDP uniquely fixes the Q^2 dependence of $F_2^{ep}(x, Q^2)$ for $\eta(W^2, Q^2) \ll 1$, a measurement of $\Lambda^2_{sat}(W^2)$ for $\eta(W^2, Q^2) \gg 1$ determines the structure function in the saturation limit of $\eta(W^2, Q^2) \ll 1$, compare the (Q^2, W^2) plane in fig. 3.

With respect to saturation, our approach of the CDP differs significantly from the point of view frequently put forward in the literature: therein, the proportionality of the structure function $F_2(x, Q^2) \sim \alpha_s(Q^2) x g(x, Q^2)$ is *assumed to persist* in the limit of $W^2 \to \infty$ with $Q^2 = \text{const}$, or $x \to 0$, leading to an infinite rise of $F_2(x, Q^2)$ for $x \to 0$ at Q^2 fixed. Non-linear effects in the gluon-distribution function [16], [17] associated with quark splitting and recombination, must then be invoked to obtain agreement with experiment.

Such an approach ignores the long life time, or the long longitudinal distance involved in the interaction of a $\gamma^* \to q\bar{q}$ fluctuation correctly contained in the CDP. Saturation according to the CDP corresponds to a transition from a proportionality to $\Lambda^2_{sat}(W^2)$ to a logarithmic dependence on this one and the same function, $\Lambda^2_{sat}(W^2)$, when passing from $\eta(W^2, Q^2) \gg 1$ to $\eta(W^2, Q^2) \ll 1$. This transition is traced back to the different interplay, for $\mu(W^2, Q^2) \gg 1$ and $\mu(W^2, Q^2) \ll 1$, between the two interaction paths of fig. 6 corresponding to the color-gauge-invariant dipole interaction (2.13).

2.5 Color Dipole Picture: Quantitative Representation of the Photoabsorption Cross Section.

The CDP yields a remarkably simple form for the photoabsorption cross section, essentially an interpolation between the general $1/\eta(W^2, Q^2)$ and $\ln(1/\eta(W^2, Q^2))$ dependences

[4]The quantity ρ yields the longitudinal-to-transverse ratio of the respective photoabsorption cross sections, $R = 1/2\rho$, for $\eta(W^2, Q^2) \gg 1$. The ratio $\rho \gtrsim 4/3$ [9] gives the relative transverse sizes of transversely-versus-longitudinally polarized $q\bar{q}$ dipole states in the color-transparency limit (2.16).

given in (2.18). For details we refer to refs. [6, 9]. The closed explicit expression (for $\rho = 1$) reads

$$\begin{aligned}\sigma_{\gamma^* p}(W^2, Q^2) &= \frac{\alpha R_{e^+e^-}}{3\pi}\sigma^{(\infty)}(W^2) I_0(\eta(W^2, Q^2)) \\ &\times \frac{\frac{\xi}{\eta(W^2,Q^2)}}{1+\frac{\xi}{\eta(W^2,Q^2)}} + O\left(\frac{m_0^2}{\Lambda^2_{\rm sat}(W^2)}\right) \end{aligned} \tag{2.21}$$

where

$$\frac{\frac{\xi}{\eta(W^2,Q^2)}}{1+\frac{\xi}{\eta(W^2,Q^2)}} \cong \begin{cases} 1, & \text{for } \eta(W^2,Q^2) \ll \xi = 130 \\ \frac{\xi}{\eta(W^2,Q^2)}, & \text{for } \eta(W^2,Q^2) \gg \xi = 130 \end{cases} \tag{2.22}$$

and $I_0(\eta(W^2, Q^2))$ is given by

$$\begin{aligned} I_0(\eta(W^2,Q^2)) &= \frac{1}{\sqrt{1+4\eta(W^2,Q^2)}} \ln \frac{\sqrt{1+4\eta(W^2,Q^2)}+1}{\sqrt{1+4\eta(W^2,Q^2)}-1} \cong \\ &\cong \begin{cases} \ln \frac{1}{\eta(W^2,Q^2)} + O(\eta \ln \eta), & \text{for } \eta(W^2,Q^2) \to \frac{m_0^2}{\Lambda^2_{\rm sat}(W^2)}, \\ \frac{1}{2\eta(W^2,Q^2)} + O\left(\frac{1}{\eta^2}\right), & \text{for } \eta(W^2,Q^2) \to \infty \end{cases} . \end{aligned} \tag{2.23}$$

The hadronic dipole-proton cross section, $\sigma^{(\infty)}(W^2)$, in (2.21) is determined by requiring consistency of (2.21) with $Q^2 = 0$ photoproduction.

$$\sigma^{(\infty)}(W^2) = \frac{3\pi}{\alpha R_{e^+e^-}} \frac{1}{\ln \frac{\Lambda^2_{sat}(W^2)}{m_0^2}} \begin{cases} \sigma^{Regge}_{\gamma p}(W^2), \\ \\ \sigma^{PDG}_{\gamma p}(W^2). \end{cases} . \tag{2.24}$$

In (2.24), $\sigma^{Regge}_{\gamma p}(W^2)$ asymptotically grows as a small power of W^2 in distinction from $\sigma^{PDG}_{\gamma p}(W^2)$ that grows as $(\ln W^2)^2$. For the explicit expressions for these photoproduction cross sections, we refer to refs. [9, 18].

The parameter ξ, empirically determined as $\xi \cong 130$, restricts the masses of $q\bar{q}$ fluctuations, $M_{q\bar{q}}$, via $M^2_{q\bar{q}} \leq m_1^2(W^2) = \xi \Lambda^2_{sat}(W^2)$. With $m_0^2 = 0.15 GeV^2, \Lambda^2_{sat}(W^2) = C_1 (W^2/1GeV^2)^{C_2}$, where $C_1 = 0.34 GeV^2$ and $C_2 \cong 0.27$ to 0.29, one obtains the theoretical results shown in fig. 2.

2.6 The Neutrino-Nucleon Cross Section in the CDP.

Finally, I come back to the neutrino-nucleon cross section to be predicted at ultrahigh energies. Inserting the expression for $F_2^{ep}(x, Q^2)$, or rather the photoabsorption cross section (2.21) of the CDP, into the expression for the neutrino-nucleon cross section (2.1), we find [18]

$$\begin{aligned}\sigma_{\nu N}(E) &= \frac{G_F^2 M_W^4}{8\pi^3 \alpha} \frac{n_f}{\sum_q Q_q^2} \int_{Q^2_{Min}}^{s-M_p^2} dQ^2 \frac{Q^2}{(Q^2+M_W^2)^2} \\ &\times \int_{M_p^2}^{s-Q^2} \frac{dW^2}{W^2} \frac{1}{2}(1+(1-y)^2) \sigma_{\gamma^* p}(\eta(W^2,Q^2)). \end{aligned} \tag{2.25}$$

Upon numerical evaluation of (2.25), based on the photoabsorption cross section from Section 2.5, we find the results shown in fig. 7 [18].

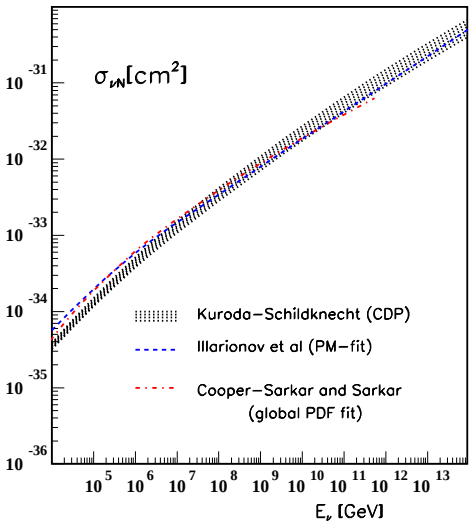

Figure 7: The prediction [18] of the neutrino-nucleon cross section from the CDP. For comparison, we also show the results based on the pQCD improved parton model fit, the "global PDF fit", to the HERA experimental data. The PM-fit is a convenient parameterization of the global PDF fit.

The shaded area in fig. 7 corresponds to a change of the exponent C_2 between $C_2 = 0.27$ and $C_2 = 0.29$. In fig. 7, we see that our prediction, based on a small number of parameters, essentially C_1 and C_2 to determine $\Lambda^2_{sat}(W^2)$ supplemented by the bounds m_0^2 and $m_1^2(W^2) = \xi\Lambda^2_{sat}(W^2)$ on the actively contributing $q\bar{q}$ dipole states, coincide with the very elaborate pQCD fits to the HERA data, the global PDF fit, obtained by the big pQCD collaborations with a huge number of fairly arbitrary fit parameters. The results of the PM fit in fig. 6 are based on a six-arbitrary-parameter fit to the global PDF fit for the parton distribution functions at low x.

2.7 Comparison with the Froissart-inspired Ansatz.

As early as in 1953, Heisenberg [19] considered the question of the behavior of cross sections among strongly-interacting particles at asymptotically high energies. Picturing the proton as a Lorentz-contracted sphere with exponentially decreasing edge, and requiring a minimum blackness necessary for particle production to occur, he predicted an increase of strong-interaction cross sections with energy as $(\ln(W^2))^2$. In 1961, it was shown by Froissart [20] that a growth as $(\ln W^2)^2$ is the maximum growth allowed by unitarity and analyticity in quantum field theory.

In a series of papers by Block et al [21] - [24], it was recently shown that a hadron-like "Froissart-inspired" ansatz of the form $F_2^{ep}(x,Q^2) \sim \sum_{n,m=0,1,2} a_{nm}(\ln Q^2)^n(\ln(1/x))^m$, with seven free fit parameters provides an excellent representation of the low-x DIS data

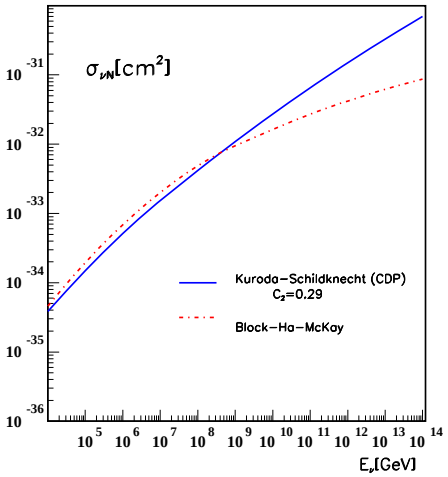

Figure 8: Comparison [18] of the predictions from the CDP with the results from the "Froissart-inspired" ansatz.

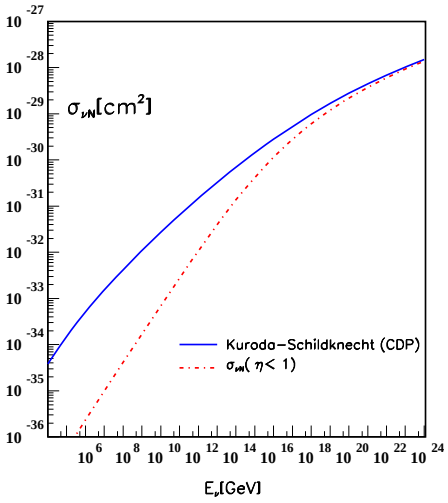

Figure 9: The neutrino-nucleon cross section compared [18] with the part of this cross section that is due to the saturation region characterized by the kinematic constraint of $\eta(W^2, Q^2) < 1$.

from HERA. The prediction for ultrahigh-energy neutrino scattering [23], based on employing in (2.1) with (2.6) the Froissart-inspired ansatz, is shown in fig. 8. There is satisfactory agreement with the predictions from the CDP (and accordingly with the predictions from the pQCD-improved parton model) for energies up to $E \lesssim 10^8$GeV $= 100$PeV, two orders of magnitude above the energy of the recently observed IceCube events.

The Froissart-inspired ansatz, according to fig. 8, for energies $E \gtrsim 10^8$GeV implies a weaker growth with energy than the prediction from the CDP. The CDP, according to (2.21) with (2.23) and $\sigma_{\gamma p}^{PDG}(W^2)$ in (2.24), in the saturation region of $\eta(W^2, Q^2) \ll 1$ contains the same Froissart-like $(\ln W^2)^2$ behavior as the Froissart-inspired approach.

The differences in fig. 8 must accordingly be due to the differences in the Q^2 dependences between these two approaches. According to the CDP, as shown in fig. 9, at energies even far beyond $E \cong 10^8$GeV, for energies below $E \cong 10^{12}$GeV, the contribution to the neutrino-nucleon cross section from the saturation region of $\eta(W^2, Q^2) < 1$ is suppressed by at least one order of magnitude. Contributions from the $(\ln W^2)^2$ behavior in the saturation region only start to dominate the neutrino-nucleon cross section at unrealistic ultra-ultrahigh energies beyond the upper end of $E \cong 10^{12}$GeV of the cosmic-ray spectrum in fig. 1.

Our results from the CDP differ significantly from various results in the literature incorporating non-linear evolution effects [16] in the pQCD improved parton-model-approach. The results imply [25, 26, 5, 27] neutrino cross sections that at $E \cong 10^{12}$GeV are approximately a factor of two to three below our predictions in figs. 7 and 8.

3 Conclusions

Inspired by cosmic-neutrino-search experiments, we thoroughly examined the neutrino-nucleon cross section at ultrahigh energies. Our results, based on the simple closed analytic expression for the photoabsorption cross section at low x in the CDP, in the full range of energies $E \lesssim 10^{12}$GeV, are consistent with the results based on the extrapolation of the elaborate multi-parameter global pdf fits to the HERA experimental data.

Below energies of $E \lesssim 10^8$GeV, two orders of magnitude above the energy $E \approx 10^6$GeV of the recently detected IceCube events, our CDP results also agree with the predictions from the Froissart-inspired approach to DIS.

Above energies of $E \gtrsim 10^8$GeV, the predictions from the CDP disagree with both, the predictions from the Froissart-inspired approach, and the predictions incorporating non-linear evolution of parton-distribution functions. These predictions lead to a suppressed cross section, when compared with the CDP, the suppression reaching factors of approximately three at $E \approx 10^{12}$GeV.

The CDP-based analysis shows that the ultrahigh-energy neutrino-nucleon cross section, in the full range of energies, up to $E \approx 10^{12}$GeV, of the cosmic-ray spectrum, is dominated by contributions from the kinematic region, where color transparency determines the interaction. The dominance of color transparency is responsible for the consistency of the CDP neutrino-nucleon cross section with the global pdf fits, while excluding the presence of screening effects due to non-linear evolution.

Acknowledgement

The author thanks Kuroda-san for fruitful collaboration on the color dipole picture.

It is a great pleasure for the author to thank Professor Antonino Zichichi for the invitation to the 52nd Course of the International School of Subnuclear Physics with the lively scientific atmosphere in the magnificent environment of the Ettore Majorana Foundation and Centre for Scientific Culture at Erice, Sicily.

References

[1] W. Bietenholz, arXiv:1305.1346 [physics.hist-ph]

[2] L.A. Anchordoqui, V. Barger et al.
arXiv:1312.6587 [astro-ph.HE], JHEAp 1-2 (2014)1.

[3] L.A. Anchordoqui, V. Barger et al.
arXiv: 1404.0622 [hep-ph]

[4] S.L. Glashow
Phys. Rev. 118 (1960) 316.

[5] V.P. Goncalves and P. Hepp
Phys. Rev. D83 (2011) 014014.

[6] D. Schildknecht, in *Diffraction 2000, Cetraro, Italy, September 2-7, 2000*, Nucl. Phys. B, Proc. Supplement 99 (2001) 121;
D. Schildknecht, B. Surrow, M. Tentyukov, Phys. Lett. B499, 116 (2001);
G. Cvetic, D. Schildknecht, B. Surrow, M. Tentyukov, EPJC 20, 77 (2001)

[7] B. Gorczyca, D. Schildknecht, Phys. Lett. 47B (1973) 71;
J.J. Sakurai, Phys. Lett. B46 (1973) 207;
J.J. Sakurai, in *Laws of Hadronic Matter, 1973 Internat. School of Subnuclear Physics, Erice, Sicily* (ed. A. Zichichi, Academic Press, New York) p. 291;
D. Schildknecht and F. Steiner, Phys. Lett. B56, 36 (1975);
E. Poggio, H.P. Quinn, S. Weinberg, Phys. Rev. D13, 1958 (1976);
M. Genovese, N.N. Nikolaev, B.G. Zakharov, Phys. Lett. B380, 213 (1996);
A.D. Martin, M.R. Ryskin, T. Teubner, Phys. Rev. D55, 4329 (1997).

[8] D. Schildknecht, in *DIS 2001, The 9th International Workshop on Deep Inelastic Scattering, Bologna, Italy, 2001*, G. Brassi et al. (Eds.), World Scientific, Singapore, 2002, p. 798;
D. Schildknecht, B. Surrow and M. Tentyukov, Mod. Phys. Lett. A16 (2001) 1829.

[9] M. Kuroda and D. Schildknecht, Phys. Rev. **D85** (2012) 094001.

[10] J.J. Sakurai and D. Schildknecht, Phys. Lett. **40B** (1972) 121; ibid **41B** (1972) 489; ibid **42B** (1972) 216;
B. Gorczyca, D. Schildknecht, Phys. Lett. **47B** (1973) 71;
H. Fraas, B.J. Read and D. Schildknecht, Nucl. Phys. **B86** (1975) 346;
R. Devenish and D. Schildknecht, Phys. Rev. **D19** (1976) 93.

[11] D. Schildknecht, in *Proc. of Photon 2005, Int. Conf. on the Structure and Interaction of the Photon*, Warsaw 2005; Acta Phys. Polon. B **37** (2006) 595.

[12] N.N. Nikolaev, B.G. Zakharov, Z. Phys. C49, 607 (1991).

[13] G. Cvetic, D. Schildknecht, A. Shoshi, Eur. Phys. J C13, 301 (2000).

[14] C. Ewerz und O. Nachtmann, Ann. Phys. **322** (2007) 1635; **322** (2007) 1670.

[15] D. Schildknecht, in *What we would like LHC to give us, 2012 International School of Subnuclear Physics, Erice-Sicily, June 23-July 2, 2012*, ed. A. Zichichi (World Scientific 2014), pp. 45-65, also published in Modern Physics Letters A Vol. 29, **No. 25** (2014) 1430028

[16] I. Balitzki, Nucl. Phys. **B463** (1996) 99,
Yu. V. Kovchegov, Phys. Rev. **D60** (1999) 034008; ibid **D61** (2000) 074018.

[17] J. Kuokkanen, K. Rummukainen and H. Weigert, arXiv: 1108.1867, Nucl. Phys. **A875** (2012) 29.

[18] M. Kuroda, D. Schildknecht, arXiv:1305.0400
Phys. Rev. **D88** (2013) 053007.

[19] W. Heisenberg, *Vorträge über kosmische Strahlung* (Springer, Berlin, 1953), p. 155, reprinted in W. Heisenberg, *Collected Works, Series B* (Springer, Berlin,1984) p.498; Die Naturwissenschaften **61** (1974), 1, reprinted in *Collected Works, Series B*, p. 912.

[20] M. Froissart, Phys. Rev. **123** (1961) 1053. .

[21] M.M. Block, E. Berger and C.-I. Tan, Phys. Rev. Lett **97** (2006) 252003;
E. Berger, M. Block and C.-I. Tan, Phzs. Rev. Lett **98** (2007) 242001.

[22] E. Berger, M.M. Block, D. McKay and C.-I. Tan, Phys. Rev. **D77** (2008) 053007.

[23] M.M. Block, P. Ha and D. McKay, Phys. Rev. **D82** (2010) 077302.

[24] M.M. Block, L. Durand, P. Ha, D.W. McKay, arXiv:1302.6119v2 [hep-ph], Phys. Rev. **D88** (2013) 014006.
M.M. Block, L. Durand, P. Ha, D.W. McKay, arXiv:1302.6127v1 [hep-ph], Phys. Rev. **D88** (2013) 013003.

[25] K. Kutak, J. Kwiecinski, arXiv: hep-ph/0303209, Eur. Phys. J. **C29** (2003) 521.

[26] M.H. Reno, arXiv: hep-ph/0410109, Nucl. Phys. Proc. Suppl. **143** (2005) 407.

[27] M.V.T. Machado, arXiv: 1112.0555 [hep-ph], Int. J. Mod. Phys. Proc. Suppl. **E20** (2011) 189.